PCCP

Accepted Manuscript

ROYAL SOCIETY OF CHEMISTRY

www.rsc.org/pccp

Understanding the degradation mechanism of rechargeable lithium/sulfur cells: a comprehensive study of the sulfur-graphene oxide cathode after discharge/charge cycling

Xuefei Feng,[‡a,b], Min-Kyu Song,[‡c,d] Wayne C. Stolte,[b,e] David Gardenghi,[b,e] Duo Zhang,[b,f] Xuhui Sun,[f] Junfa Zhu,*[a] Elton J. Cairns,*[d,g] and Jinghua Guo*[b,h]

a. National Synchrotron Radiation Laboratory & Collaborative Innovation Center of Suzhou Nano Science and Technology, University of Science and Technology of China, Hefei 230029, China.

b. Advanced Light Source, Lawrence Berkeley National Laboratory, Berkeley, CA 94720, USA.

c. The Molecular Foundry, Lawrence Berkeley National Laboratory, Berkeley, CA 94720, USA

d. Department of Chemical and Biomolecular Engineering, University of California, Berkeley, CA 94720, USA

e. Department of Chemistry, University of Nevada, Las Vegas, NV 89154-4003, USA

f. Institute of Functional Nano & Soft Materials (FUNSOM), Soochow University, Suzhou 215123, Jiangsu, China

g. Environmental Energy Technologies Division, Lawrence Berkeley National Laboratory, Berkeley, CA 94720, USA

h. Department of Chemical and Biochemistry, University of California, Santa Cruz, CA 95064, USA

Keywords: *sulfur-graphene oxide, lithium/sulfur cells, capacity fading, scanning electron microscopy, near edge X-ray absorption fine structure, X-ray photoelectron spectroscopy.*

ABSTRACT: Lithium/sulfur (Li/S) cells have attracted much attention due to their higher theoretical specific capacity and energy compared to those of current lithium-ion cells. However, the application of Li/S cells is still hampered by short cycle life. Sulfur-graphene oxide (S-GO) nanocomposites have shown promise as cathode materials for long-life Li/S cells because oxygen-containing functional groups on the surface of graphene oxide were successfully used as sulfur immobilizer by forming weak bonds with sulfur and polysulfides. While S-GO showed much improved cycling performance, the capacity decay still needs to be improved for commercially viable cells. In this study, we attempt to understand the capacity fading mechanism by *ex-situ* studying the structural and chemical evolution of S-GO nanocomposites cathode with various numbers of cycles using scanning electron microscopy (SEM), near edge X-ray absorption fine structure (NEXAFS) and X-ray photoelectron spectroscopy (XPS). It is found that both the surface morphologies and chemical structures of the cathode materials change considerably with increasing number of cycles. These changes are attributed to several unexpected chemical reactions of lithium with S-GO nanocomposites occurred during the discharge/charge processes with the formation of Li_2CO_3, Li_2SO_3, Li_2SO_4, and $COSO_2Li$ species. These reactions result in the loss of recyclable active sulfur on the surface of the electrode, and thus capacity fades while coulombic efficiency is near 100%. Moreover, the reaction products accumulate on the cathode surface, forming a compact blocking insulating layer which may make the diffusion of Li ions into/out of the cathode difficult during the discharge/charge process and thus lead to lower utilization of sulfur at higher rates. We think that these two observations are significant contributors to the capacity and rate capability degradation of the Li/S-GO cells. Therefore, for the rechargeable Li/S-GO cells, we suggest that the content of oxygen-containing functional groups on GO should be optimized and more stable functional groups need to be identified for further improvement of the cycling performance. The information we gain from this study may provide general insights into the fundamental understanding of the degradation mechanisms for other rechargeable Li/S cells using similar oxygen-containing functional groups as sulfur immobilizers.

1. Introduction

Although Li-ion cells are still considered as "state-of-the-art" technology amongst many existing cells on the market, it is questionable whether they are able to meet tomorrow's energy storage requirements for advanced transportation and portable electronics.[1-5] Current cathode materials such as $LiCoO_2$ and $LiFePO_4$ have exhibited good cycling performance so far; however, their obtain-

able specific energies are insufficient to meet the ever-increasing demands of the rapidly emerging advanced technologies.[3,6] In contrast, sulfur (S) is a very attractive material for use as a cathode in rechargeable lithium batteries with high specific energy thanks to its high theoretical specific capacity of 1675 mAh/g and high theoretical specific energy (with lithium) of 2600 Wh/kg. However, despite these technical merits, the practical application of Li/S cells is still hindered by their low coulombic efficiency and short cycle life.[7-14] One key reason for the short cycle life and low coulombic efficiency was attributed to the formation of the lithium polysulfides and the dissolution of these polysulfides into the organic solvent electrolytes during the discharge/charge process, which leads to low utilization and the loss of so-called "recyclable" active sulfur material (sulfur that can react reversibly with lithium during the cycling process, $2Li + xS \leftrightharpoons Li_2S_x$, $1 \leq x < 8$) in the cathode.[15-19] In recent years, conductive polymers and various carbon materials have been widely used for accommodating S to mitigate the issues related to the loss of sulfur, as reported by Nazar, et al. and the others.[20-30] For instance, sulfur-graphene oxide (S-GO) nanocomposites produced via a chemical approach were used as the cathode material of the Li/S cell and a high reversible capacity of 950-1400 mA h g^{-1} for more than 50 cycles has been achieved.[22] More recently, we reported that a Li/S cell employing a cetyltrimethyl ammonium bromide (CTAB)-modified sulfur-graphene oxide (S–GO) nanocomposite cathode can be discharged at rates as high as 6C (1C = 1.675 A/g of sulfur) and charged at rates as high as 3C while still maintaining high specific capacity (~ 800 mA·h/g of sulfur at 6C), with a long cycle life exceeding 1500 cycles and an extremely low decay rate (0.039% per cycle), perhaps the best performance demonstrated so far for a Li/S cell.[28] The CTAB was thought to protect the outer layer of sulfur from dissolving and the elastomeric SBR/CMC binder might maintain the integrity of the electrode structure. Even though, the capacity fading (~60 % after 1500 cycles) is still the main obstacle for further improving the cell cycle life. Therefore, it's of great importance to deeply understand why the capacity fades upon cycling through analyzing the structural evolution of the cathode materials at different discharge/charge cycles.

In our previous works, we have studied the structure and morphology of pure S-GO material before cycling.[22,31] The results suggested that the carbon rings and oxygen-containing functional groups (such as hydroxyl, epoxide, carbonyl and carboxyl groups) of GO form chemical bonds with sulfur, which helps to immobilize S atoms on the GO surface and thus reduce the shuttle phenomenon. In this work, we report a comprehensive ex-situ investigation of the morphological and structural evolution of the S-GO based cathode used in the Li/S cell before and after various numbers of discharge/charge cycles by scanning electron microscopy (SEM), total electron yield and total fluorescence yield near edge X-ray absorption fine structure (TEY- and TFY- NEXAFS) and X-ray photoelectron spectroscopy (XPS). Here we use S-GO instead of CTAB-modified S-GO to eliminate the impact of CTAB, as the C-S bonds may also form between S and CTAB.[28] We have demonstrated that the surface morphological/chemical structural changes of S-GO nanocomposite cathode after discharge/charge process are significant factors that influence the cell performance. The information we gain here may provide a general insight towards fundamental understanding of the degradation mechanisms of the Li/S cells and will be helpful for the optimal design of novel cathode materials.

2. Experimental procedures

2.1. Synthesis and characterization of S-GO nanocomposites

0.36 g sodium sulfide (Na_2S, anhydrous, Alfa Aesar) was dissolved in 25 ml ultrapure water (Millipore®) to form a Na2S solution, followed by adding 0.45 g elemental sulfur (S, sublimed, 99.9%, Mallinckrodt) and stirring with a magnetic stirrer for 2 hours at room temperature to obtain a sodium polysulfide (Na_2S_x) solution. In the meantime, 18 ml of commercial graphene oxide (GO) dispersed in deionized (DI) water (10 mg/ml, ACS Material) was taken by an auto pipette and diluted with ultrapure water (162 ml) to form a uniform GO suspension (180 mg GO in 180 ml ultrapure water). Next, the Na_2S_x solution was added to the prepared GO suspension dropwise using a glass pipette while stirring, followed by further stirring for an additional 16 hours. The as-prepared Na_2S_x-GO blended solution was then slowly added to 100 ml of formic acid (HCOOH, 88%, Aldrich, 2 M) using a burette while vigorously stirring. This mixture was stirred for half an hour to allow elemental S to be precipitated onto the GO. Finally, the S-GO nanocomposite was filtered and washed with acetone and ultrapure water multiple times to remove salts and impurities. The S-GO nanocomposite was then dried at 50 ^{o}C in a vacuum oven for 24 hours. Thereafter, the as-synthesized S-GO nanocomposite was heat treated in a tube furnace under flowing argon with a flow rate of 100 cc/s at 155 ^{o}C for 12 hours. Thermo gravimetric analysis (TGA, TA Instruments Q5000) was used to determine the weight of the sulfur deposited onto the GO using a heating rate of 10 ^{o}C/min in N_2. The TGA weight loss to 600 ^{o}C was found to be approximately 50 wt %. A detailed description of the S-GO morphology can be found in the previous studies.[22,31] Briefly, a uniform deposition of a thin sulfur film on GO can be observed without substantial agglomeration of sulfur. This is important to achieving a high utilization by providing a short diffusion distance for lithium atoms and a better electronic conductivity.

2.2. Electrode fabrication and electrochemical characterization

The sulfur electrodes were prepared by ultrasonically mixing the S-GO nanocomposite and a conductive carbon black additive (Super P) with PVDF binder at a weight ratio of 70:20:10 in N-methyl-2-pyrrolidone (NMP) forming a uniform slurry. The resulting slurry was spread using a doctor blade onto an aluminum foil. The NMP sol-

vent was allowed to evaporate at room temperature for 24 hours. The electrodes were then dried in a vacuum oven at 50 °C for 48 hours to fully eliminate any residual solvent. The electrode was punched into 12.7 mm diameter circular pieces for cell assembly. The average sulfur loading of the electrodes was ~0.7 mg/cm^2. For the electrolyte, a mixture of 1,3-dioxolane (DOL) and dimethoxyethane (DME) was introduced to ionic liquid, (n-methyl-n-butyl) pyrrolidinium bis(trifluoromethanesulfonyl)imide ($PYR_{14}TFSI$, Sigma-Aldrich), to form a 1 M LiTFSI in $PYR_{14}TFSI$/DOL/DME solution (2:1:1 by volume). The electrolyte also contained 0.1 M $LiNO_3$ as an additive.

CR2032-type coin cells were assembled by sandwiching two separators (Celgard 2400) between lithium metal foil (99.98%, Cyprus Foote Mineral) and a sulfur electrode (area=1.26 cm^2) fabricated with the S-GO nanocomposite in an argon glove box. Galvanostatic discharge and charge cycling between 1.5 V and 2.8 V was performed using a battery cycler (Maccor Series 4000). The cell capacity was normalized to the weight of sulfur (based on the TGA weight loss to 600°C). Before all electrochemical characterizations, the cells were held at open circuit at room temperature for 24 h. All electrochemical characterizations were performed inside a test chamber (TestEquity TEC1) maintained at 30 °C.

2.3. Observation of structural changes of electrodes by scanning electron microscopy

Five Li/S-GO cells with the same initial structures were assembled and discharged/charged at the rate of 1 C and 0.25 C (1 C = 1675 mA/g of sulfur), respectively. Note that all cathodes were examined after the cells were charged up to 2.8 V vs. Li/Li$^+$. After 1, 10, 30, 50 or 100 cycles, the Li/S cells were disassembled inside a glove box filled with high-purity argon gas, followed by the separation of lithium metal anodes and the rinsing of the sulfur cathodes with a DOL/DME mixture (1:1 by volume). Thereafter, the cathode materials, which are a combination of S-GO, carbon black (super P) and poly(vinylidene fluoride) (PVDF) binder, were dried inside the antechamber attached to the glove box for 30 minutes under vacuum. Through these treatments, the salts (for example, LiTFSI) in the electrolyte and possibly a small amount of high-order polysulfides that may remain on the S-GO cathode surface was removed, enabling us to better investigate the evolution of chemical bonding between S and GO after discharge/charge cycles. For comparison, a sulfur cathode without prior cycling was also prepared. A scanning electron microscope (SEM, Zeiss Gemini Ultra-55) was operated at an accelerating voltage of 3 kV to examine the morphology of the S-GO nanocomposite electrodes before and after cycling.

2.4. Total electron yield (TEY) and total fluorescence yield (TFY) NEXAFS experiments

Before the NEXAFS experiments, six samples (pristine and after 1, 10, 30, 50, 100 cycles) were transferred into chambers under the protection of argon gas and then the chambers were pumped down immediately. The NEXAFS experiments were carried out at two separate beam lines at the Advanced Light Source (ALS), Lawrence Berkeley National Laboratory (LBNL). The S K-edge data were collected at a bending magnet beam line 9.3.1 with photon energies ranging from 2320 to 5600 eV and an unfocused beam size of 1 mm × 0.7 mm. A silicon drift detector was equipped for TFY measurements and the TEY signals were recorded by measuring the sample drain current. The C K-edge and O K-edge measurements were acquired at the undulator beamline 8.0.1. This beamline consists of a 5 cm period undulator with photon energies ranging from 80 eV to 1250 eV. The TEY signal was obtained by monitoring the sample drain current. The TFY signals at the Beamline 8.0.1 were collected by a channeltron. The energy resolutions were approximately 0.36 eV for the S K-edge, and 0.1 eV for the C K-edge and O K-edge measurements. The photon incident angle was set to be 45º for all samples.

2.5. X-ray photoelectron spectroscopic characterization

The XPS experiments on the same samples were carried out on a VG MARK II spectrometer, which has been described in detail elsewhere.[32] All the samples are protected by argon before the measurements. This spectrometer comprises three ultrahigh vacuum (UHV) chambers: analysis chamber, preparation chamber and scanning tunneling microscope (STM) chamber. The base pressures of the three chambers are 4×10^{-11} mbar, 3×10^{-11} mbar and 2×10^{-11} mbar, respectively. For S 2p measurements, the Mg Kα source (hν = 1253.6 eV) was chosen and the overall energy resolution was 0.9 eV. Note that all the XPS data were collected at normal emission and the binding energies of the peaks were referenced to the Au 4f of a clean Au(111) single crystal.

3. Results

3.1. Cycling Performance of S-GO nanocomposite cathodes

Initially, the nanostructured S-GO composite cathodes made with a PVDF binder exhibited a specific capacity of 1115 mAh/g of sulfur at the 0.05 C rate and a good utilization of 863 mAh/g of sulfur at the 1 C rate, as shown in Figures 1a and 1b, respectively. This electrode can be successfully cycled in the ionic liquid-based electrolyte up to 100 cycles at a rate of 1 C and 0.25 C for discharge and charge, respectively, with a high coulombic efficiency of near 100% (Figure 1a). We used a slower charge rate than discharge rate as we found that how the Li/S cells are charged can notably affect the cycle life and coulombic efficiency. We will report these results in a separate publication. After the first discharge/charge cycle, the cycling performance of the S-GO composite electrode became stable at 1 C and exhibited better capacity retention after the noticeable initial loss (-11.6%). The average decay rate per cycle for 100 cycles was -0.14% (or 86.6% capacity retention) after the 2nd cycle and -0.23% (or 76.5% capacity retention) including the 1st cycle. To check the specific

capacity that can be obtained at a lower C-rate, discharge capacity was measured using the 0.05 C rate. After 100 cycles at 1 C/0.25 C discharge/charge, the S-GO nanocomposite cathodes exhibited a discharge capacity of 920 mAh/g of sulfur at 0.05 C (83% capacity retention with respect to the initial 1115 mAh/g of sulfur at 0.05 C), showing the promise of the S-GO nanocomposite as a cathode material for high energy rechargeable Li/S cells (Figure 1b). As can be seen in Figure 1a and 1b, although the coulombic efficiency can be kept high, the capacity still fades with increasing the number of cycles. Therefore, we need a deep fundamental understanding of degradation mechanism in order to further improve the cycling performance for commercially viable cells.

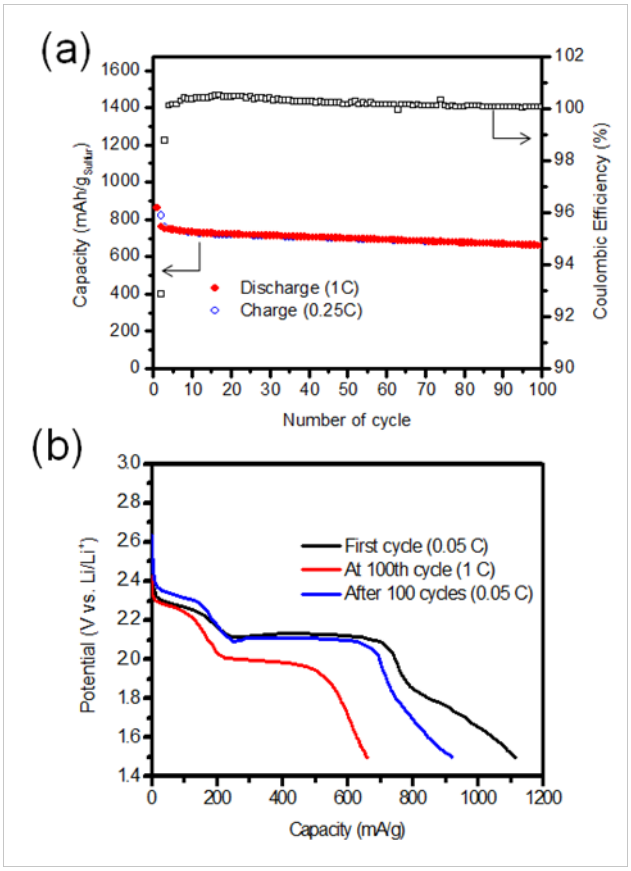

Figure 1. (a) Capacity and coulombic efficiency evolution of S-GO based Li/S cells, (b) Discharge profiles at initial discharge and after 100 cycles of Li/S cells with S-GO nanocomposite cathodes.

3.2. Structural/Morphological changes in sulfur electrodes

To understand the capacity fading mechanism of such Li/S-GO cells, we have first carried out SEM experiments to investigate the morphological evolution of the S-GO composite electrodes after different numbers of discharge/charge cycles, and the results are shown in Figure 2. The layer-like conjugated nanostructures with highly developed porous structures of pure S-GO was described in detail in the previous studies.[22,31] Here, the SEM image of the original S-GO cathode (before cycling) was also shown as a reference. As can be seen in Figure 2a, the original S-GO cathode has a porous structure with a well-mixed morphology of S-GO and carbon black. After the first discharge/charge cycle, the porous materials become a little smoother compared to the initial sample, as shown in Figure 2b. With increasing numbers of cycles, the morphology of the cathode material surface becomes smoother and smoother, as seen in the SEM images of the cathode material with 10, 30, 50 and 100 cycles (Figure 2c-f). It can be seen that the initial porous surface turns from sharp to blurry and the edges of S-GO are attached by membranous materials. In particular, after 100 cycles, remarkable morphological changes can be observed: (1) the sharp S-GO pieces in the cathode disappear and the edges of the S-GO nanocomposite become much smoother; (2) the macro-porous structure of the cathode becomes less porous. As the large contact area of electrolyte/cathode can shorten the transport lengths for both lithium ions and electrons, which helps to improve the overall electrochemical performance,[22,33] one can imagine that the cell cycle performance can be strongly influenced by the change of S-GO nanocomposite morphology. In general, the morphology evolution is usually associated with the changes of surface chemical structure. However, these SEM images do not provide any chemical information about the surfaces. In order to gain information about the chemical changes upon discharge/charge cycles, we have performed a parallel set of NEXAFS and XPS experiments on the electrodes, which will be presented below.

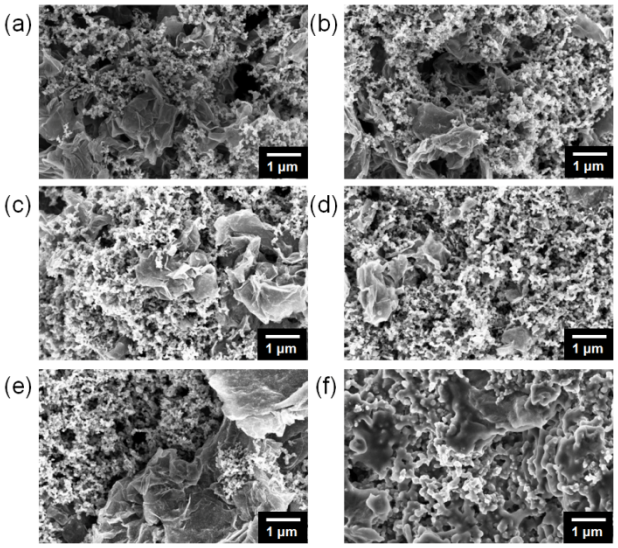

Figure 2. SEM images of S-GO nanocomposite electrodes consisting of S-GO, PVDF binder and carbon black: (a) before and after (b) 1, (c) 10, (d) 30, (e) 50 and (f) 100 cycles. All electrodes were examined in the fully charged state.

3.3. NEXAFS characterization of sulfur electrodes

NEXAFS, based on the excitation of core electrons to empty or partially filled states, is a powerful technique for probing the electronic band structure of materials.[34,35] In

addition, NEXAFS spectra recorded with different detection modes such as total electron yield (TEY) and total fluorescence yield (TFY), different probing depths can be achieved. The TEY mode probes a depth of ~5 nm, whereas the TFY mode probes a depth of ~100 nm. Here we employed both TEY- and TFY-NEXAFS experiments to explore the evolution of the electronic and chemical structures of S-GO electrode materials after the discharge/charge process. Figure 3a displays the S K-edge TEY-NEXAFS spectra of the cathode materials after six different numbers of cycles (labeled as 0, 1, 10, 30, 50 and 100). For comparison, the TEY S K-edge absorption spectrum of pure S-GO and the TFY signal from the cathode before cycling are presented as the top two lines, respectively. For the initial S-GO composite cathode (0 cycle), several absorption features can be observed. According to the previous studies,[31,36-43] the feature at 2472.2 eV can be attributed to the transition from the S 1s core level to the S-S π* states of elemental S or C-S-S-C π* states of S-GO, and the strong absorption feature at 2473.7 eV corresponds to the transition from the S 1s to the C-S σ* of S-GO species.[36,37,42] The results can be confirmed by the comparison of the TEY spectra of pure elemental S and S-GO, as shown in Figure S1. In addition, the fairly weak and wide peak around 2480.5 eV is assigned to the S 1s transition to the $COSO_2^-$ σ*, while the S 1s transition to SO_4^{2-} σ* is located at 2482.5 eV.[39] One may notice a small peak at 2470.2 eV, which is related to chemical bonding between S atoms and GO sheets. However, the correlation of this peak to a specific transition is still an open question so far. By comparing the spectra of the TEY mode and the TFY mode from the 0 cycle sample, one can notice that the ratio between the peaks at 2472.2 eV and 2473.7 eV in the TFY mode is higher than that in the TEY spectrum. Because the probing depth of the TEY mode is smaller than that of the TFY mode, this lower intensity of the 2472.2 eV feature in the TEY spectrum implies less elemental S or C-S-S-C species near the electrode surface. In contrast, the stronger 2473.7 eV peak in TEY spectra indicates that there are more C-S species located on the cathode surface than in the bulk after cell assembling.

Upon cycling, three significant changes in the S K-edge TEY-NEXAFS spectra can be found with increasing number of cycles: (1) intensity decay of the peaks at 2470.2, 2472.2 and 2473.7 eV; (2) appearance of a new peak at 2478.0 eV; (3) intensification of the two peaks located at 2480.5 and 2482.5 eV. Note that all of the measured spectra are from fully charged S-GO cathodes, thus, the evolution of the spectra directly reflects the reversibility of the cathode structure as a result of cycling. The significant decay of the three peaks at 2470.2, 2472.2 and 2473.7 eV implies the loss of elemental S and/or S species bonded to GO, i.e., active S species, as a result of cycling. The new peak at 2478.0 eV can be assigned to the transition of S 1s to S^{2-} σ* and/or SO_3^{2-} σ*.[37,38] For the 2480.5 eV peak, at first thought it may originate from the LiTFSI, the S K-edge of which shows a strong absorption peak at 2480.5 eV (see Figure S2), left on the cathode surface during sample preparation. However, this salt also contains N element, but no N signal can be found in the N K-edge spectra (spectrum not shown), indicating that the peak at 2480.5 eV should be attributed to the $COSO_2^-$ species.[42] In addition, the peak at 2482.5 eV can be assigned to S 1s transition to σ* of SO_4^{2-}.[36] The appearance and increase of $COSO_2^-$ and SO_4^{2-} species in the cathode after cycling further confirms that they originate at the expense of active S species. One may argue that lithium also possibly react with LiTFSI during cycling. However, according to the literature, this reaction is very weak.[44] Moreover, our S-GO cathodes were rinsed with DOL/DME mixture many times to avoid the influence of the sulfur-containing lithium salt. Thus, we attribute most of the reaction products to the reaction between Li and S-GO.

The C K-edge spectra shown in Figure 3b further reveal remarkable changes in the chemical structure of the electrode materials after cycling. As can be seen, before cycling, three distinct features located at 285.5, 287.6 and 292.0 eV can be observed. Comparing to the study on pure S-GO nanocomposites and other carbon related materials,[31,45,46] the strong 285.5 eV peak can be assigned to the C 1s transition to π* of GO and/or carbon black, and the 287.6 eV peak is attributed to the transition from C 1s to C-H and C-S σ*. Moreover, the peak around 292.0 eV corresponds to transitions from the 1s level to dispersionless σ* states at the Γ point of the graphene Brillouin zone (BZ).[31,47] After cycling, significant changes in the C K-edge spectra with increasing numbers of cycles can be observed: (1) the damping of peak at 285.5 eV; (2) the intensity decrease of the 287.6 eV feature; (3) the development of two new features located at 288.7 and 290.6 eV. According to the previous study on lithium oxalate, lithium succinate and lithium methoxide by Augustsson et al.,[48] the 288.7 eV peak can be assigned to the transition of C 1s level to the σ* of $-CH_2-$ species, while the peak at 290.6 eV can be ascribed to the C 1s transition to CO_3^{2-} and RO^- σ*. After 100 cycles, the 290.6 eV peak becomes the strongest peak in the spectra. These results imply the formation of lithium carboxylate (for example, Li_2CO_3) and possible lithium alkoxide during Li/S-GO cell operation. To understand more about the reaction products after the unexpected chemical reactions, further theoretical calculation is needed.

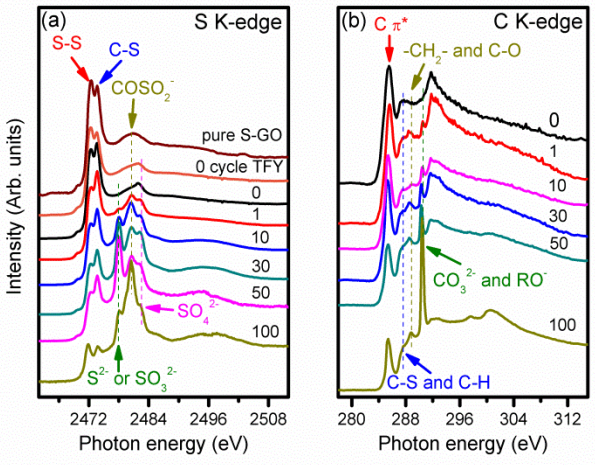

Figure 3. NEXAFS spectra of S K-edge (a), C K-edge (b) of the S-GO cathode materials at different discharge/charge cycles. The top two lines in (a) show the spectra of the TEY signal from pure S-GO and TFY signal from the cathode materials before cycling. All the samples were examined in the fully charged state and the characteristic peaks of different functional groups are indicated in the figures.

To further understand the changes in chemical structure of the cathode materials after cycling, the S K-edge and C K-edge spectra are deconvoluted with Gaussian-functions after subtracting an arctan function background. Representative spectrum deconvolutions for S K-edge and C K-edge of S-GO nanocomposite cathode are presented in Figures 4a and 4b, respectively. These spectra are obtained from the cathode material after 30 cycles. All the peak assignments have been described above. By normalizing to the total integrated area of each spectrum, the relative intensity of each sulfur-containing species as a function of the number of cycles is shown in Figure 4c. As seen, the continuous decrease of S-S/S-C bonds with increasing cycles indicates the significant loss of active sulfur species in S-GO or residual S on the cathode surface. In contrast, the contents of SO_3^{2-}, $COSO_2^-$, SO_4^{2-} species increase, implying that the strong chemical reactions of lithium with sulfur and the oxygen-containing functional groups in S-GO occur, leading to the formation of lithium sulfite, lithium sulfate and other lithium-sulfur compounds. Judging from the intensity variation of the C-S feature (2473.7 eV feature in S K-edge spectra) after 100 cycles, about 65% of the C-S species gets lost.

The evolution of different C species, shown in Figure 4d, in the C K-edge spectra further confirms the reaction of Li ions with the functional groups in S-GO cathode. The decrease of C π* (red line) implies the strong interaction between lithium ions and the conjugated structure of GO or carbon black, while the content reduction of C-S bonds (blue line) indicates some of the C-S bonds disappear due to the occurrence of strong chemical reactions between lithium and functional groups in GO together with sulfur during the discharge/charge process. In addition, with increasing number of cycles, the lithium carbonate species are progressively formed.

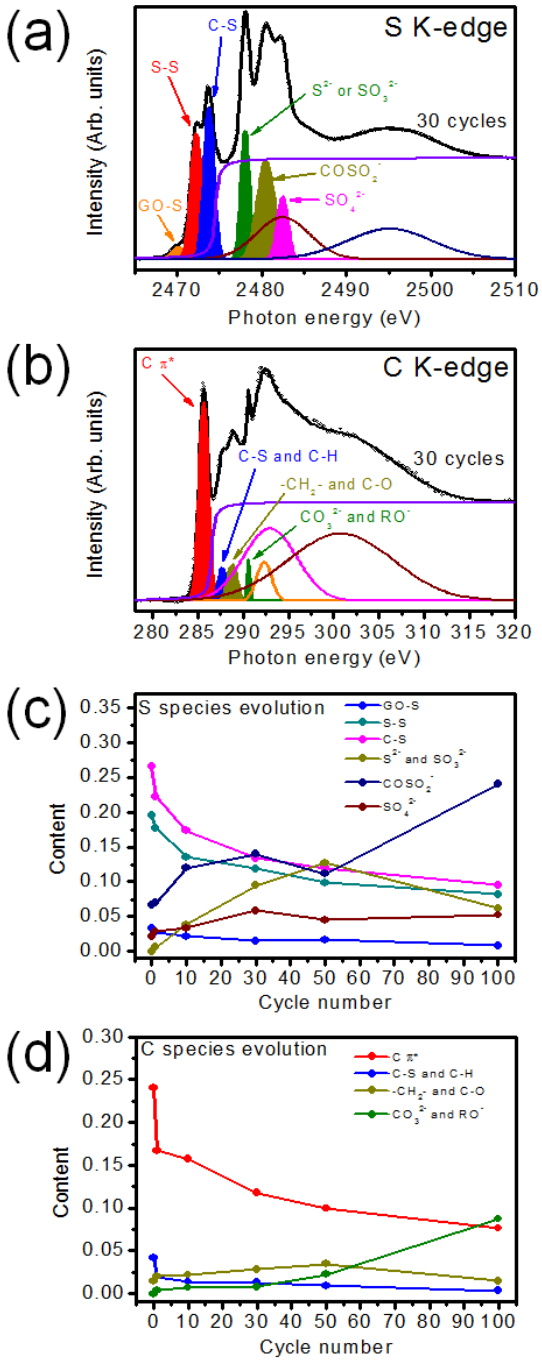

Figure 4. Representative NEXAFS peak fittings for S K-edge (a) and C K-edge (b) of the cathode materials after subtracting an arctan background. The spectra were obtained after 30 cycles. The black open circles are the experimental data. Individual components together with their assignments are labeled with different colors. The evolutions of each S and C species as a function of the number of discharge/charge cycles are plotted in (c) and (d), respectively. All electrodes were examined in the fully charged states.

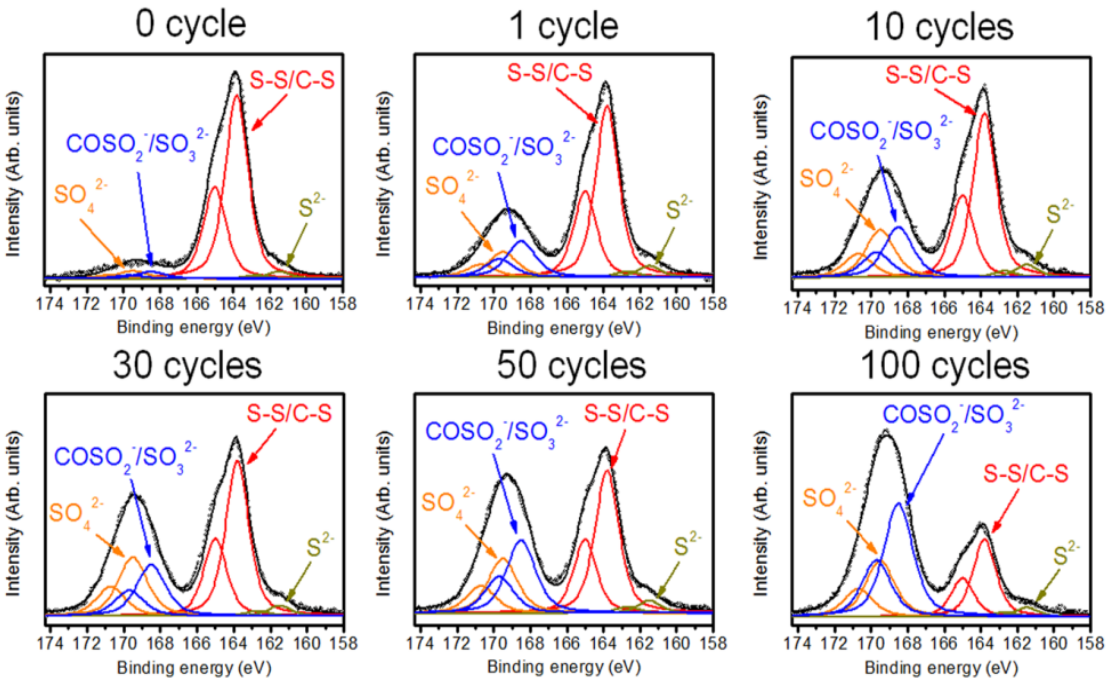

Figure 5. S 2p spectra together with their peak fittings from the cathode materials after 0, 1, 10, 30, 50 and 100 cycles. Each individual component corresponds to a different functional group, as indicated in the figures. The black open circles represent the experimental data. All the samples were examined in the fully charged state.

This is further supported by the evolution of O K-edge spectra with different cycles (see Figure S3). As shown, significant peak shape changes of O K-edge spectra can be observed. The detailed peaks assignments are given in the supporting information. Together with above observations of S K-edge and C-edge, we can conclude that during discharging, Li can diffuse into the cathode and react with both the S-O functional groups and the oxygen-containing functional groups on GO sheets to form Li2SO3 and Li2SO4 species on the cathode surface. On the other hand, strong chemical reactions between Li and carboxyl on GO sheets can also occur, leading to the formation of Li2CO3 species.

Note that the above-described evolution of S K-edge and C K-edge spectra are from the TEY signals. For comparison, the bulk-sensitive TFY signals are also acquired and the results are presented in Figure S4. Significantly, the peak intensities of CO_3^{2-}, SO_3^{2-}, SO_4^{2-} and $COSO_2^-$ features are lower than those of the TEY spectra at the same cycles, indicating that the reaction products mainly accumulate on the cathode surface.

3.4. XPS spectroscopy characterization of S-GO nanocomposite cathode

XPS is another powerful surface-sensitive technique for probing the chemical structure of materials. To validate the chemical reactions between Li and S-GO during cycling, S 2p measurements on the same samples were carried out. As shown in Figure 5, before cycling, the strong S $2p_{3/2}$ peak at 163.8 eV is attributed to the active S species with S-S/C-S bonds in S-GO and possible residual S after heat treatment,[31,36] while the weak S $2p_{3/2}$ feature at 161.5 eV can be ascribed to the S^{2-} of residual Na_2S during the chemical synthesis process.[31] In addition, two weak S $2p_{3/2}$ peaks at 168.5 eV and 169.5 eV are also observed, which can be assigned to the $COSO_2Li/Li_2SO_3$ and Li_2SO_4 species, respectively.[36,49,50] It should be mentioned that these two peaks may be also from the sulphate species formed by oxidation of sulfur.[31,36,51] After 1 cycle, the damping of the S $2p_{3/2}$ at 163.8 eV as well as the intensification of the 168.5 eV and 169.5 eV peaks can be observed, implying that strong chemical reactions occur between Li ions diffused into the cathode and S-GO during the discharge/charge process. After more cycles, further damping of S 2p of S-GO species is found together with the increase in the intensities of S 2p of Li_2SO_3, $COSO_2Li$ and Li_2SO_4. After 100 cycles, only about 25% of the active S species (the peak of 163.8 eV) in S-GO remain on the cathode surface. This result coincides very well with the above TEY-NEXAFS results. Therefore, the combination of XPS and NEXAFS measurements provides a strong evidence that part of the low valence S coverts to high oxidation state S during discharge/charge cycling, leading to the loss of recyclable active S, which can be one of the key reasons for the capacity fading.

4. Discussion

As described above, we have comprehensively investigated both the morphological and chemical evolution of the S-GO cathode materials in real cell operating environments with various numbers of discharge/charge cycles. For the SEM images of S-GO cathode surface with different cycles, there are two dominant observations that should be rationalized:

(1) The original sharp edges of S-GO nanocomposite in the cathode become smoother and the surface of S-GO

are covered by dense membranous materials after cycling. Especially for the sample after 100 cycles, the highly developed layer-like structure of S-GO can be hardly observed.

(2) After discharge/charge cycles, the cathode material surface becomes less porous.

On the other hand, key chemical structure evolution of the S-GO cathode was obtained from our NEXAFS and XPS experiments:

(1) The S K-edge spectra combined with C K-edge results indicate the loss of recyclable active S in S-GO as well as the appearance of Li_2CO_3, Li_2SO_3, Li_2SO_4, $COSO_2Li$ species in the cathode materials after cycling. XPS spectra strongly confirm the NEXAFS results.

(2) By comparing the TEY spectra of S K-edge and C K-edge with TFY signals, we demonstrate that these reacted lithium compounds mainly accumulate on the cathode surface.

Combined with the electrochemical results, we propose an explanation that is consistent with the above observations to understand the relation between the cycle performance of Li/S-GO cell and the morphological/chemical structures of the cathode materials:

Firstly, the strong GO-S chemical interaction can help to reduce the dissolution of the lithium polysulfides into the electrolyte and thus minimize the shuttle phenomenon.[22] Therefore, the coulombic efficiency can be kept as high as nearly 100% with very low capacity decay rate (-0.14% per cycle for 100 cycles after 2nd cycle). However, the functional groups in GO, together with sulfur, can react strongly with lithium during the discharge/charge process, leading to the loss of recyclable active sulfur materials in the cathode. This can be the immediate cause for the capacity fading while the decay rate can be minimized using oxygen-containing functional groups on the surface of GO.

Secondly, as the structure of the cathode material is critical to the cycle performance of rechargeable lithium batteries,[9,22,52-56] the cycle performance of the Li/S-GO cell

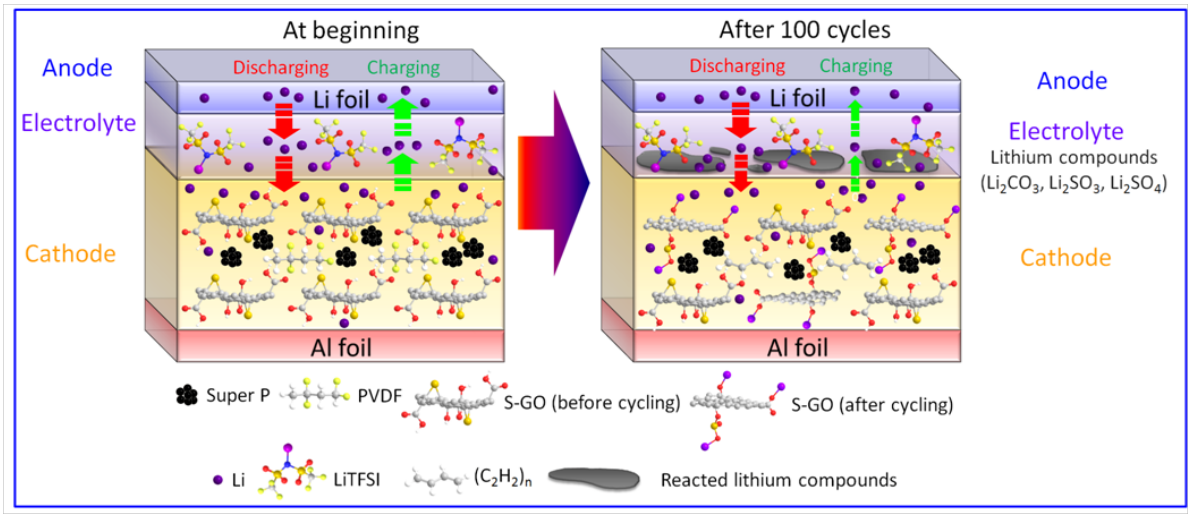

Figure 6. Schematic illustration of the discharge/charge process for Li/S-GO battery.

is significantly influenced by the accumulation of these lithium compounds on the cathode surface: (i) after cycling, the less porous structure of the cathode cannot accommodate the large volume change of S any more, leading to the possible mechanical degradation of the cathode and the particles of disintegrated sulfur may be more vulnerable to dissolution in the electrolyte; (ii) these lithium compounds are electrical insulators. Thus, the deposition of such reaction products on the cathode surface can reduce the in-depth discharge of sulfur, leading to low utilization of sulfur especially at higher rates. As a result, the Li/S-GO cell capacity fades with the increase of such reaction products; (iii) the intimate contact of S provided by the large surface area and the functional groups on GO is favorable to good electron/ion accessibility. However, when the porous S-GO cathode surface is covered by these reacted lithium compounds, not only the surface area of S-GO is reduced but also the contact between diffused lithium ions and sulfur during discharging is prevented, leading to the cycle performance degradation.

Summarizing the SEM, NEXAFS, XPS results and the analysis above, we have demonstrated that besides the supposed electrochemical reaction of $2Li + xS \rightarrow Li_2S_x$, the unexpected strong chemical reactions between lithium and the oxygen-containing functional groups on GO and immobilized sulfur also occur on the S-GO cathode surface, leading to the loss and lower utilization of recyclable active sulfur materials in the cathode with increasing cycles. A simplified model is proposed to describe the discharge/charge process of Li/S-GO cell, as schematically shown in Figure 6. At the first several cycles, Li ions diffuse into the cathode to react with S-GO during discharging. Thereafter, most of the Li ions can move back to the lithium electrode during charging. This can be proved by our NEXAFS and XPS spectra that only a small amount of unexpected reaction products (i.e., SO_3^{2-}, SO_4^{2-} species) can be found. With increasing number of cycles, more

and more unexpected reaction products appear and accumulate on the cathode surface, leading to the formation of a lithium compound blocking layer at the electrolyte/electrode interface. Therefore, during the discharge/charge process, the diffusion of Li ions into and out of the cathode becomes increasingly difficult and the expected electrochemical reactions between Li and S atoms are progressively hindered. As a result, the overall capacity fading is found in the electrochemical cycling tests.

The above results suggest that although the oxygen-containing functional groups on GO can help to immobilize S atoms on GO and improve the initial cycling performance of Li/S cells, they can also strongly react with lithium, leading to the loss of recyclable active sulfur material in S-GO and the formation and accumulation of Li_2CO_3, Li_2SO_3, Li_2SO_4, and $COSO_2Li$ insulating layers on the cathode surface that result in the reduction of in-depth discharge of sulfur as well as the mechanical degradation of the cathode. Moreover, same phenomena will be expected even if the S loading is increased in the cathode because the chemical process taking place on S-GO composite cathodes during cycling is expected to be the same. Therefore, in order to further improve the Li/S-GO cell cycle stability, the content of oxygen-containing functional groups on GO should be optimized to both increase the interaction of S with GO and minimize the unexpected chemical reactions. In addition, more stable functional groups as sulfur immobilizers need to be identified for further improving the cycle performance. On the other hand, we strongly suggest that when introducing new materials, such as conducting polymers, porous carbon materials and metal oxides, as S immobilizers, the interaction of Li and these materials should be taken into account. We expect that this new degradation mechanism we proposed in this study can be also helpful for understanding why the capacity fades in the other Li/S cells.

ASSOCIATED CONTENT

Supporting Information

S K-edge comparison of S_8/S-GO (TEY); S K-edge (TEY) of LiTFSI; O K-edge (TEY) evolution of S-GO cathode with increasing number of cycles; TFY signals for S K-edge and C K-edge of S_GO cathode. This material is available free of charge via the Internet at http://pubs.acs.org.

AUTHOR INFORMATION

Corresponding Author

jfzhu@ustc.edu.cn; ejcairns@lbl.gov; jguo@lbl.gov;

Author Contributions

‡These authors contributed equally.

ACKNOWLEDGMENT

J.F.Z greatly acknowledges the financial support from the National Basic Research Program of China (2010CB923302, 2013CB834605), the National Natural Science Foundation of China (Grant No. U1232102), and the Specialized Research Fund for the Doctoral Program of Higher Education of Ministry of Education (Grant No. 20113402110029). E.J.C. thanks for financial support from the University of California, Office of the President, under the Proof of Concept Grant No. 12PC247581. The work at the Advanced Light Source is supported by the Office of Science, the Office of Basic Energy Sciences and the U.S. Department of Energy under Contract No. DE-AC02-05CH11231.

REFERENCES

(1) Bruce, P. G.; Freunberger, S. A.; Hardwick, L. J.; Tarascon, J.-M. *Nature Materials* **2012**, *11*, 19.

(2) Armand, M.; Tarascon, J. M. *Nature* **2008**, *451*, 652.

(3) Song, M.-K.; Park, S.; Alamgir, F. M.; Cho, J.; Liu, M. *Materials Science and Engineering: R: Reports* **2011**, *72*, 203.

(4) Goodenough, J. B.; Park, K. S. *Journal of the American Chemical Society* **2013**, *135*, 1167.

(5) Ji, X. L.; Lee, K. T.; Nazar, L. F. *Nature Materials* **2009**, *8*, 500.

(6) Ellis, B. L.; Lee, K. T.; Nazar, L. F. *Chemistry of Materials* **2010**, *22*, 691.

(7) Song, M.-K.; Cairns, E. J.; Zhang, Y. *Nanoscale* **2013**, *5*, 2186.

(8) Lin, T. Q.; Tang, Y. F.; Wang, Y. M.; Bi, H.; Liu, Z. Q.; Huang, F. Q.; Xie, X. M.; Jiang, M. H. *Energy & Environmental Science* **2013**, *6*, 1283.

(9) Weng, W.; Pol, V. G.; Amine, K. *Advanced Materials* **2013**, *25*, 1608.

(10) Yin, L. C.; Wang, J. L.; Lin, F. J.; Yang, J.; Nuli, Y. *Energy & Environmental Science* **2012**, *5*, 6966.

(11) Xiao, L. F.; Cao, Y. L.; Xiao, J.; Schwenzer, B.; Engelhard, M. H.; Saraf, L. V.; Nie, Z. M.; Exarhos, G. J.; Liu, J. *Advanced Materials* **2012**, *24*, 1176.

(12) Cai, K. P.; Song, M. K.; Cairns, E. J.; Zhang, Y. G. *Nano Letters* **2012**, *12*, 6474.

(13) Ji, X. L.; Evers, S.; Black, R.; Nazar, L. F. *Nature Communications* **2011**, *2*. 1293.

(14) He, G.; Ji, X. L.; Nazar, L. *Energy & Environmental Science* **2011**, *4*, 2878.

(15) Akridge, J. R.; Mikhaylik, Y. V.; White, N. *Solid State Ionics* **2004**, *175*, 243.

(16) Kumaresan, K.; Mikhaylik, Y.; White, R. E. *Journal of the Electrochemical Society* **2008**, *155*, 576.

(17) Mikhaylik, Y. V.; Akridge, J. R. *Journal of the Electrochemical Society* **2004**, *151*, 1969.

(18) Yamin, H.; Gorenshtein, A.; Penciner, J.; Sternberg, Y.; Peled, E. *Journal of the Electrochemical Society* **1988**, *135*, 1045.

(19) Shim, J.; Striebel, K. A.; Cairns, E. J. *Journal of the Electrochemical Society* **2002**, *149*, 1321.

(20) Liang, C. D.; Dudney, N. J.; Howe, J. Y. *Chemistry of Materials* **2009**, *21*, 4724.

(21) Choi, Y. J.; Chung, Y. D.; Baek, C. Y.; Kim, K. W.; Ahn, H. J.; Ahn, J. H. *Journal of Power Sources* **2008**, *184*, 548.

(22) Ji, L. W.; Rao, M. M.; Zheng, H. M.; Zhang, L.; Li, Y. C.; Duan, W. H.; Guo, J. H.; Cairns, E. J.; Zhang, Y. G. *Journal of the American Chemical Society* **2011**, *133*, 18522.

(23) Zu, C.; Manthiram, A. *Advanced Energy Materials* **2013**. 1008.

(24) Cao, Y.; Li, X.; Aksay, I. A.; Lemmon, J.; Nie, Z.; Yang, Z.; Liu, J. *Physical Chemistry Chemical Physics* **2011**, *13*, 7660.

(25) Wang, H.; Yang, Y.; Liang, Y.; Robinson, J. T.; Li, Y.; Jackson, A.; Cui, Y.; Dai, H. *Nano Letters* **2011**, *11*, 2644.

(26) Evers, S.; Nazar, L. F. *Accounts of Chemical Research* **2013**, *46*, 1135.
(27) Yang, Y.; McDowell, M. T.; Jackson, A.; Cha, J. J.; Hong, S. S.; Cui, Y. *Nano Letters* **2010**, *10*, 1486.
(28) Song, M.-K.; Zhang, Y.; Cairns, E. J. *Nano Letters* **2013**, *13*, 5891.
(29) Lu, S. T.; Cheng, Y. W.; Wu, X. H.; Liu, J. *Nano Letters* **2013**, *13*, 2485.
(30) Seh, Z. W.; Li, W. Y.; Cha, J. J.; Zheng, G. Y.; Yang, Y.; McDowell, M. T.; Hsu, P. C.; Cui, Y. *Nature Communications* **2013**, *4*, 2327.
(31) Zhang, L.; Ji, L.; Glans, P.-A.; Zhang, Y.; Zhu, J.; Guo, J. *Physical Chemistry Chemical Physics* **2012**, *14*, 13670.
(32) Chen, M.; Feng, X. F.; Zhang, L.; Ju, H. X.; Xu, Q.; Zhu, J. F.; Gottfried, J. M.; Ibrahim, K.; Qian, H. J.; Wang, J. O. *Journal of Physical Chemistry C* **2010**, *114*, 9908.
(33) Yu, Y.; Chen, C. H.; Shi, Y. *Advanced Materials* **2009**, *21*, 3541.
(34) Cuisinier, M.; Cabelguen, P. E.; Evers, S.; He, G.; Kolbeck, M.; Garsuch, A.; Bolin, T.; Balasubramanian, M.; Nazar, L. F. *Journal of Physical Chemistry Letters* **2013**, *4*, 3227.
(35) Liu, X. S.; Wang, D. D.; Liu, G.; Srinivasan, V.; Liu, Z.; Hussain, Z.; Yang, W. L. *Nature Communications* **2013**, *4*, 3568.
(36) Ota, H.; Akai, T.; Namita, H.; Yamaguchi, S.; Nomura, M. *Journal of Power Sources* **2003**, *119*, 567.
(37) Takeuchi, T.; Kageyama, H.; Nakanishi, K.; Tabuchi, M.; Sakaebe, H.; Ohta, T.; Senoh, H.; Sakai, T.; Tatsumi, K. *Journal of the Electrochemical Society* **2010**, *157*, 1196.
(38) Takeuchi, T.; Kageyama, H.; Nakanishi, K.; Inada, Y.; Katayama, M.; Ohta, T.; Senoh, H.; Sakaebe, H.; Sakai, T.; Tatsumi, K.; Kobayashi, H. *Journal of the Electrochemical Society* **2012**, *159*, 75.
(39) Dey, A.; Chow, M.; Taniguchi, K.; Lugo-Mas, P.; Davin, S.; Maeda, M.; Kovacs, J. A.; Odaka, M.; Hodgson, K. O.; Hedman, B.; Solomon, E. I. *Journal of the American Chemical Society* **2006**, *128*, 533.
(40) Totir, D. A.; Antonio, M. R.; Schilling, P.; Tittsworth, R.; Scherson, D. A. *Electrochimica Acta* **2002**, *47*, 3195.
(41) Ouvrard, G.; Wu, Z. Y. *Nuclear Instruments & Methods in Physics Research Section B-Beam Interactions with Materials and Atoms* **1997**, *133*, 120.
(42) Schmalenberger, A.; Pritzkow, W.; Ojeda, J. J.; Noll, M. *International Biodeterioration & Biodegradation* **2011**, *65*, 1215.
(43) Baturina, O. A.; Gould, B. D.; Korovina, A.; Garsany, Y.; Stroman, R.; Northrup, P. A. *Langmuir* **2011**, *27*, 14930.
(44) Ensling, D.; Stjerndahl, M.; Nyten, A.; Gustafsson, T.; Thomas, J. O. *Journal of Materials Chemistry* **2009**, *19*, 82.
(45) Mkhoyan, K. A.; Contryman, A. W.; Silcox, J.; Stewart, D. A.; Eda, G.; Mattevi, C.; Miller, S.; Chhowalla, M. *Nano Letters* **2009**, *9*, 1058.
(46) Jeong, H. K.; Noh, H. J.; Kim, J. Y.; Jin, M. H.; Park, C. Y.; Lee, Y. H. *Epl* **2008**, *82*, 67004.
(47) Lee, V.; Whittaker, L.; Jaye, C.; Baroudi, K. M.; Fischer, D. A.; Banerjee, S. *Chemistry of Materials* **2009**, *21*, 3905.
(48) Augustsson, A.; Herstedt, M.; Guo, J. H.; Edstrom, K.; Zhuang, G. V.; Ross, P. N.; Rubensson, J. E.; Nordgren, J. *Physical Chemistry Chemical Physics* **2004**, *6*, 4185.
(49) Ota, H.; Sato, T.; Suzuki, H.; Usami, T. *Journal of Power Sources* **2001**, *97-8*, 107.
(50) Lu, M.; Cheng, H.; Yang, Y. *Electrochimica Acta* **2008**, *53*, 3539.
(51) Schaufuss, A. G.; Nesbitt, H. W.; Kartio, I.; Laajalehto, K.; Bancroft, G. M.; Szargan, R. *Journal of Electron Spectroscopy and Related Phenomena* **1998**, *96*, 69.
(52) Bensch, W.; Ophey, J.; Hain, H.; Gesswein, H.; Chen, D.; Monig, R.; Gruber, P. A.; Indris, S. *Physical Chemistry Chemical Physics* **2012**, *14*, 7509.
(53) Lytle, J. C.; Yan, H. W.; Ergang, N. S.; Smyrl, W. H.; Stein, A. *Journal of Materials Chemistry* **2004**, *14*, 1616.
(54) Yang, Y.; Yu, G. H.; Cha, J. J.; Wu, H.; Vosgueritchian, M.; Yao, Y.; Bao, Z. A.; Cui, Y. *Acs Nano* **2011**, *5*, 9187.
(55) Ding, F.; Xu, W.; Graff, G. L.; Zhang, J.; Sushko, M. L.; Chen, X. L.; Shao, Y. Y.; Engelhard, M. H.; Nie, Z. M.; Xiao, J.; Liu, X. J.; Sushko, P. V.; Liu, J.; Zhang, J. G. *Journal of the American Chemical Society* **2013**, *135*, 4450.
(56) Guo, J. C.; Xu, Y. H.; Wang, C. S. *Nano Letters* **2011**, *11*, 4288.

Table of contents (TOC) Graphic instructions: